Time-Resolved ATR-FTIR Spectroscopy of the Oxygen Reaction in the D124N Mutant of Cytochrome *c* Oxidase from *Paracoccus denitrificans*†

Elena A. Gorbikova, Nikolai P. Belevich, Mårten Wikström, and Michael I. Verkhovsky*

Structural Biology and Biophysics Program, Institute of Biotechnology, PB 65 (Viikinkaari 1), FIN-00014 University of Helsinki, Helsinki, Finland

Received August 10, 2007; Revised Manuscript Received September 18, 2007

ABSTRACT: Real-time measurements of the cytochrome *c* oxidase reaction with oxygen were performed by ATR-FTIR spectroscopy, using a mutant with a blocked D-pathway of proton transfer (D124N, *Paracoccus denitrificans* numbering). The complex spectrum of the ferryl→oxidized transition together with other bands showed protonation of Glu 278 with a peak position at 1743 cm^{-1}. Since our time resolution was not sufficient to follow the earlier reaction steps, the FTIR spectrum of the CO-inhibited fully reduced→ferryl transition was obtained as a difference between the spectrum before the laser flash and the first spectrum after it. A trough at 1735 cm^{-1} due to deprotonation of Glu 278 was detected in this spectrum. These observations confirm the proposal [Smirnova I.A., et al. (1999) *Biochemistry 38*, 6826−6833] that the proton required for chemistry at the binuclear site is taken from Glu 278 in the perroxy→ferryl step, and that the rate of the next step (ferryl→oxidized) is limited by reprotonation of Glu 278 from the N-side of the membrane in the D124N mutant enzyme. The blockage of the D-pathway in this mutant for the first time allowed direct detection of deprotonation of Glu 278 and its reprotonation during oxidation of cytochrome oxidase by O_2.

Cytochrome *c* oxidase (C*c*O[1]) is the terminal complex of the respiratory chain. C*c*O transfers electrons from cytochrome *c* to oxygen via four redox centers: Cu_A, heme *a*, heme a_3, and Cu_B. The energy released upon electron transfer is used for proton translocation. The electron-coupled proton transfer is carried out in four reaction steps, the P (peroxy)→F (ferryl), F→O_H (transient oxidized), O_H→E_H (transient one-electron-reduced), and E_H→R (reduced) transitions (for review, see ref *1*). At each of these steps the binuclear center (BNC), that consists of heme a_3 and Cu_B, accepts one electron and one proton for oxygen reduction chemistry ('chemical' proton). Moreover, one additional proton is translocated ('pumped') across the membrane at each transition (*2*).

Uptake of two 'chemical' protons in the P→F and F→O_H steps and four 'pumped' protons in all four steps of the catalytic cycle is carried out via the proton-transferring D-channel, which contains two protolytic groups: D124 located at the entrance of the channel and ∼25 Å away from Glu 278 that is positioned near the level of the hemes. The other two 'chemical' protons are taken up through the K-channel during reduction of the BNC (the O_H→E_H and E_H→R transitions) (*1*). This basic scheme predicts a key role of Glu 278 in relaying protons to be pumped, or to be consumed at the BNC (*3*, *4*).

The role of Glu 278 in proton transfer was proposed on the basis of the crystal structure (*5*) and confirmed by site-directed mutations (*6*, *7*). The role of Glu 278 in proton transfer can be easily tested in the D124N mutant enzyme where the orifice of the D-channel is blocked. In the P→F transition of this mutant, the proton for the chemistry was proposed to be taken from Glu 278, but its reprotonation via the D-channel was suggested to be slowed down dramatically (*8*), limiting all further events of catalysis.

Electron-coupled proton-transfer kinetics in cytochrome *c* oxidase has been extensively studied by real-time measurements, mainly by the electrometric technique from where the distances of proton transfer were estimated in WT and mutant enzymes and proton-transfer sites were predicted (for review see ref *1*). However, the electrometric approach cannot identify the chemical nature of proton donors and acceptors.

Fourier transform infrared (FTIR) spectroscopy has an excellent potential to capture protonation reactions within a protein. Real-time proton transfer has been successfully probed by time-resolved FTIR in several light-excitable membrane proteins, for example in bacteriorhodopsin (*9*−*11*), photosynthetic reaction centers (*12*), and rhodopsin (*13*). The time-resolved FTIR technique was earlier applied to heme-copper oxidases in CO recombination studies on fully reduced (FR) and mixed-valence forms of the enzyme (*14*−

† This work was supported by the Sigrid Jusélius Foundation, Biocentrum Helsinki, and the Academy of Finland (project numbers 200726, 44895, and 115108), E.A.G. was supported by the ISB Graduate School.

* To whom correspondence should be addressed. Phone: +358 9 19158005. Fax: +3589 19159920. E-mail: michael.verkhovsky@helsinki.fi.

[1] Abbreviations: ATR, attenuated total reflectance; BNC, binuclear center; C*c*O, cytochrome *c* oxidase; DDM, dodecyl β-D-maltoside; E_H, transient one-electron-reduced; F, ferryl-state of the BNC; FRCO, fully-reduced CO-inhibited enzyme; FTIR, Fourier transform infrared; IR, infrared; N-side, negatively charged side of membrane; O, relaxed oxidized state; O_H, transient oxidized state; P, peroxy-state; P-side, positively charged side of membrane; R, reduced state; RS, rapid-scan; WT, wild type; τ, time constant.

10.1021/bi701614w CCC: $37.00
Published on Web 10/19/2007

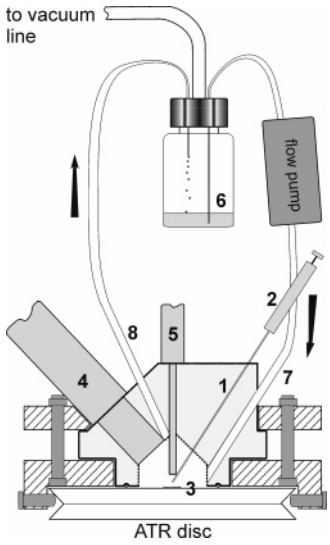

FIGURE 1: Outline of the setup for FTIR kinetics measurements of the 'ATR-sample'. ATR-chamber is tightly fit to the ATR-disc. (1) Needle for O_2-buffer injection from the syringe (*2*) that is driven by the syringe pump; (3) 'ATR-sample' of the D124N mutated C*c*O; (4) light guide from the laser; (5) light guide providing visible light to the sample and delivering reflected light to the spectrophotometer HR2000+ operating in a reflectance mode; (6) reservoir with the 'working' buffer connected to the flow pump and inlet (7) and outlet (8) of the chamber. The direction of the 'working' buffer flow during the enzyme rereduction is marked with arrows.

17), but no catalytic reaction step has been investigated up to now.

In this work we have studied the oxygen reaction in the D124N mutant of aa_3-type cytochrome oxidase from *Paracoccus denitrificans* by ATR-FTIR spectroscopy. We aimed to kinetically resolve the oxygen reaction in the mutant enzyme and to test the earlier proposal (*8*) that the binuclear center takes up a proton in the P→F step from the residue Glu 278, which is reprotonated in the next step (F→O_H) with greatly slowed velocity.

MATERIALS AND METHODS

Setup for Oxygen Reaction Measurements by ATR-FTIR. To perform kinetic measurements on C*c*O by FTIR, we constructed a setup based on the ATR (attenuated total reflectance) approach. The setup consists of an FTIR spectrometer (Bruker IFS 66/S with MCT detector) equipped with a silicon ATR prism (Sens IR Technologies, three-bounce version, surface diameter 3 mm). The design of an ATR chamber is shown in Figure 1. The needle (1) (22S RN, Hamilton, Reno, Nevada) of the syringe (2) (Hamilton, gastight, 5 mL) is directed to the center of the enzyme film (3) at a ~0.5 mm distance to produce a high local concentration of O_2 for the time of the reaction. Injection of O_2-saturated buffer by a syringe pump (SP200i, World Precision Instruments) is controlled by a timing board (Keithley MetraByte, CTM-05/A). A 100 μL amount of O_2-buffer is injected for kinetic measurements at 10 mL/min speed. The reaction of CO-inhibited fully reduced (FRCO) enzyme is initiated by a laser pulse that is delivered to the C*c*O film with a light-guide (4) (Dolan-Jenner, 0.25″ × 36″) after O_2 injection. The laser (STC, SSL MIT-51-2) pulse (~15 ns, 532 nm, ~50 mJ/cm^2) was controlled through the timing board. Control of redox state of cytochrome oxidase and measurement kinetics of absorbance changes in the visible range were achieved by the spectrophotometer HR2000+ (Ocean Optics) equipped with the light-guide (5) (Avantes, FCR-7UV200-2-1, 5 × 22, operates in a reflection mode) which was positioned on a distance of ~2 mm from the enzyme surface. After measurement of the oxygen reaction, enzyme rereduction is accelerated by the buffer flow from the reservoir (6) through the ATR-chamber. For this purpose, inlet (7) and outlet (8) of the ATR chamber were connected to a reservoir filled with 15 mL of 'working' buffer. The air in the reservoir was exchanged with 100% CO by a homemade vacuum/gas line. Pumping of the buffer was accomplished by the flow pump. The internal volume of the ATR-chamber was ~1 mL.

Oxygen injection, laser pulse, flow pump, and FTIR spectrometer were operated in an automatic mode by the timing board through TTL (transistor−transistor logic) pulses.

Preparation of 'ATR-Sample' of D124N Mutant Enzyme. Site-directed mutagenesis, bacterial growth conditions, and purification of the D124N mutant of cytochrome aa_3 from *P. denitrificans* were as described in ref *18*.

Immobilization of the mainly hydrophobic membrane protein on the hydrophobic silicon surface of the ATR-prism requires depletion of detergent. Final preparation of mutant enzyme after purification contained much more detergent compared to WT, so the procedure of preparation of the 'ATR-sample' was modified. The preparation was diluted in distilled H_2O ~70 times and concentrated in a Centricon-50 (Amicon) concentrator (*19*). This procedure was repeated several times to decrease the level of DDM. After detergent depletion, the method of Iwaki et al. was followed, essentially as described (*20*) with the exception that all buffers were replaced with 2 mM potassium phosphate at pH 6.0.

C*c*O was loaded on the ATR-prism, dried, and rewetted as described in ref *21*. The amide I intensity of semidried and rewetted enzyme was 1.2−1.7 and 0.8−1.0, respectively.

Preparation of the FRCO Form of CcO on the ATR-Prism. All experiments were carried out at pH 9.0 (buffer composition: 100 mM boric acid + 100 mM potassium sulfate) to slow down the rate of the oxygen reaction. First, the reservoir and the ATR-chamber were filled with buffer, and baselines from oxidized enzyme in visible and IR ranges were recorded. Then the buffer was changed to the 'working' one that included 100 mM glucose (Merck), 260 μg/mL catalase (Sigma), 3.3 mM ascorbate (Prolabo), and 10 μM hexaammineruthenium (III) chloride (Aldrich). The reservoir was degassed and filled with 100% CO. After that, 670 μg/mL glucose oxidase (Roche) was injected into the reservoir, and the flow pump was switched on.

Formation of the FRCO complex of the mutant enzyme was controlled by visible and FTIR spectroscopy. A sharp band at 1965 cm^{-1} appeared with full amplitude (1.8−2.7 × 10^{-3} depending on sample) within ~40 min (see Figure 3A) as well as the FRCO-minus-O (relaxed oxidized state) spectrum in the visible region (not shown). The band 1965 cm^{-1} belongs to the C≡O stretch vibration of the heme a_3−CO complex (see for example ref *22*).

Sample Quality Control. FRCO-minus-O FTIR spectra in the IR region 2200−1800 cm^{-1} were analyzed to detect the sites and the quantity of CO binding to the enzyme.

CO recombination to heme a_3 after photolysis of FRCO enzyme was followed in visible range (410−700 nm) by the spectrophotometer HR2000+ with 1 ms time resolution. Kinetics acquisition was triggered by the laser flash. Twenty to fifty kinetic absorbance surfaces for each sample were averaged and fitted by the SPLMOD algorithm (*23*, *24*) under *Matlab* operation to get the rate constant of the reaction.

CO dissociation in the dark from heme a_3 was detected using the rapid-scan (RS) mode in the 2150−1550 cm^{-1} region cut out with an interference filter. Acquisition of the spectra with ∼68 ms time resolution and 4 cm^{-1} spectral resolution was started together with 100 μL of O_2-saturated buffer injection and lasted for ∼70 s. The rate constant of the reaction was defined by fitting the averaged kinetic surface with a two-step sequential model in *Matlab* software.

To estimate the fraction of C*c*O that had bound CO to heme a_3 and that is able to react with O_2, CO photolysis from heme a_3 as the drop of amplitude at 1965 cm^{-1} after injection of O_2 that followed by a 3 s delay and the laser flash was measured. The CO photolysis was detected in the RS mode as done for the CO-dissociation experiment. The syringe for O_2-buffer injection and the reservoir containing 'working' buffer were on ice in all experiments, which slowed down the kinetics and increased the local O_2 concentration up to 2.4 mM.

Oxygen Reaction Measured by Visible Spectroscopy. The reaction was initiated by the laser pulse ∼350 ms after the beginning of the oxygen injection. By the time of the laser pulse, ∼25% of cytochrome *c* oxidase had released CO because of the increased rate of dissociation (τ ∼300 ms, data not shown) by the intensive measuring light. The absorption spectra were measured by the spectrometer HR2000+ with 1 ms resolution. Analysis of the kinetics was done by the SPLMOD algorithm in *Matlab*.

We would like to stress that visible and infrared (IR) measurements were never carried out at the same time, and when IR data were collected, visible light was switched off. All described measurements were performed on an 'ATR-sample' film.

F→O_H Transition Measurements by ATR-FTIR. Before the experiment, the amplitude of CO photolysis from heme a_3 was determined as described in *Sample Quality Control*. This amplitude was used to average sets of data from different samples and days of measurements. The data were acquired in the 1850−950 wavenumber range which was cut out by a filter (Northumbria Optical Coatings Limited). The spectra were acquired in the RS mode with ∼46 ms time resolution and 8 cm^{-1} spectral resolution. A background of 1024 coadditions was taken prior to injection of the O_2-buffer. Together with oxygen injection, RS acquisition started and was followed by a 3 s delay and the laser flash. Four hundred spectra were acquired that corresponded to ∼18.4 s. The flow pump was stopped during the background and kinetics collection. As soon as the data collection was finished, the pump was automatically switched on (1 mL/min) to accelerate C*c*O rereduction that took ∼4 min after which the pump was switched off and the cycle repeated.

All sets of data (512 'Δ absorbance-wavenumbers-time' surfaces) were normalized according to the drop in the 1965 cm^{-1} band, which was measured before and after each set and was stable during the time of experiment (∼10 h) and averaged. A global fitting procedure (by three sequential reactions, in *Matlab* software) was applied to extract the phase spectrum of the F→O_H transition.

Calculation of FRCO→F and FRCO→O_H Kinetic FTIR Spectra. Averaged sets of data were used further to calculate the spectrum of the FRCO→F transition as a difference between the spectrum obtained by the average of several time points before the laser flash and the spectrum obtained immediately after. The sum of the FRCO→F and the F→O_H spectra resulted in the kinetic FRCO→O_H spectrum.

RESULTS

Sample Quality Control. To analyze the variants of the FRCO form of the mutant enzyme, the equilibrium FRCO-minus-O spectrum was measured. The spectrum exhibited the α form of the heme a_3−CO complex with a peak position of the C≡O stretch at 1965 cm^{-1} (∼55% of the whole fraction of FRCO enzyme) (*25*), which appeared to be the main contributor in the mutant enzyme (Figure 2A). Two shoulders (at 4 cm^{-1} resolution) at ∼1975 and 1955 cm^{-1} indicate the presence of β forms (here ∼15%) (*25*, *26*). Additionally, a broad weak band at ∼2070 cm^{-1} was present and assigned to the Cu_B−CO complex (here ∼30%) (*25*). The percentages of the Cu_B−CO adduct in the D124N mutated enzyme varied depending on the preparation. In the WT 'ATR-sample' the Cu_B−CO band was present as well but with lower intensity (data not shown).

CO recombination with heme a_3 after photolysis of the FRCO form of D124N mutant enzyme occurred with a time constant (τ) of ∼17 ms, which is the same as for the WT 'ATR-sample' (data not shown) and in agreement with literature data on soluble WT enzyme from *P. denitrificans* (*27*) and *R. sphaeroides* (*28*). CO dissociation from heme a_3 in the dark was measured by the FTIR rapid scan approach and τ was determined to be ∼10 s (Figure 2B), which is very close to the WT 'ATR-sample' (not shown).

For spectral normalization and estimation of the concentration of active enzyme, CO photolysis from heme a_3 was followed by FTIR using rapid scan (Figure 2C). During the 3 s delay between the oxygen injection and the laser flash, ∼10% of the CO-inhibited enzyme had released CO and is thus not taking part in the reaction. The amplitude of the 1965 cm^{-1} band drop on photolysis was $1.1-1.7 \times 10^{-3}$. The enzyme fraction containing CO associated with Cu_B did not take part in the measured oxygen reaction because it could not be photolyzed. No CO-adduct formation was detected during ∼30 s in this experiment.

Visible Spectroscopy of the F→O_H Transition in the 'ATR-Sample'. The oxygen reaction of the D124N mutant enzyme was first measured by visible spectroscopy. Three sets of kinetic surfaces from two different samples were decomposed into component spectra. Since millisecond resolution is not sufficient to resolve the fast enzyme transitions preceding state F, only the F→O_H reaction was analyzed. Two kinetic components of the F→O_H transition were identified and had the same spectral features: the spectrum of a fast kinetic component (τ ∼35 ms) had about twice smaller amplitude than the spectrum of a slow kinetic component (τ ∼350 ms) (Figure 3). Both phases show decay of the F state characterized by the trough at around 580 nm (*29*, *30*), as well as a small fraction of heme *a* oxidation (∼10%). Although the spectra of both phases are very similar, the extent of heme

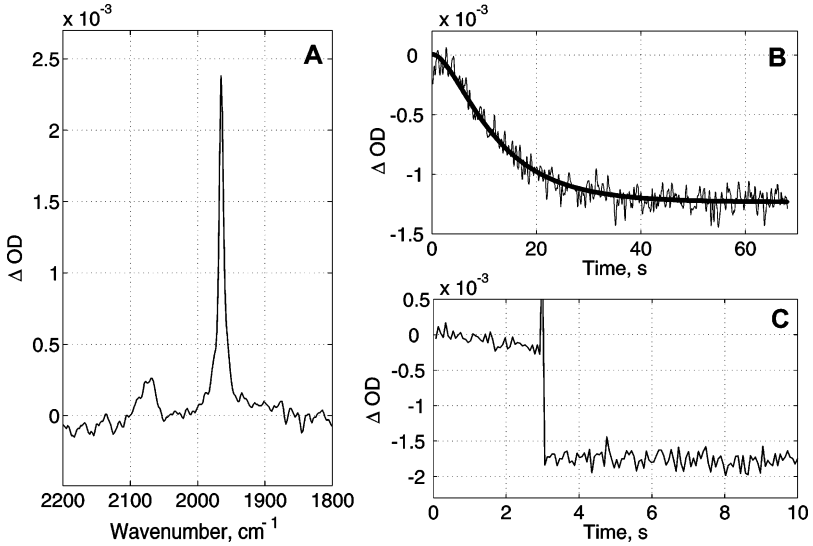

FIGURE 2: The quality control of the 'ATR-sample' of the D124N mutant enzyme for kinetic measurements. (A) FRCO-minus-O difference spectrum in the region of C≡O vibrations. The spectrum is averaged from two different samples. The main band at 1965 cm^{-1} belongs to the α-form of heme a_3−CO complex; two shoulders are from β-forms; weak broad band at ∼2070 cm^{-1} is from Cu_B−CO complex. (B) Kinetics of CO dissociation from heme a_3 at 1965 cm^{-1} is an average of four experiments from two different samples. The averaged experimental curve was fitted with two-sequential step model (thick line). The lag-phase reflects the O_2 injection and diffusion into the sample film, and the second phase is the enzyme oxidation which appears with τ of ∼10 s. (C) CO photolysis from heme a_3 at 1965 cm^{-1}. Nine surfaces from four different samples were averaged. First 10 s of the kinetics is shown.

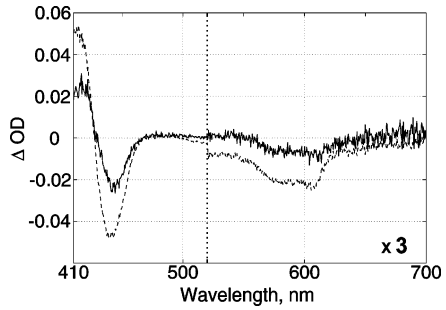

FIGURE 3: Phase spectra in visible region of two F→O_H transitions of D124N mutant enzyme. Fast phase (solid line, τ ∼35 ms) and slow phase (dashed line, τ ∼350 ms) are plotted together. The α-band region is multiplied by 3.

a oxidation is slightly higher in the fast phase as may be concluded from the red-shift of the Soret band. Notably, in the mutant enzyme, heme *a* oxidation is much smaller than in WT (∼50%) (*31*) because of smaller heme *a* reduction in the previous step of the reaction, due to uncompensated negative charge of the unprotonated Glu 278 in the F state (*8*).

F→O_H Transition by FTIR. Next, the reaction of the mutant enzyme with oxygen was followed by rapid scan FTIR spectroscopy. The FTIR data was decomposed into kinetic phases. The unresolved immediate jump after the laser flash (Figure 4 B) corresponds to the sum of all processes faster than 46 ms, which is the time resolution of the method. The first resolved phase developed with τ ∼400 ms, correlates well with the second phase of the kinetics in the visible range, and was assigned to the F→O_H transition. Note that the 400 ms FTIR F→O_H phase was well fitted with a single-exponential equation excluding heterogeneity of the enzyme population that is turning over after the laser flash. There were two more slow phases in the FTIR kinetics, which were due to artefactual migration of the contents of the 'working' buffer into the injected O_2-saturated buffer within the area of the penetration depth of the ATR crystal. The spectrum of the O_H-minus-F kinetic phase from averaged data (512 surfaces averaged) is shown in Figure 4A.

The kinetic O_H-minus-F spectrum of the D124N mutant enzyme resembles the O-minus-F spectra of WT enzyme obtained in equilibrium conditions, where H_2O_2 was used to produce the F state (*20*, *32*, *33*) but contains several additional bands. The most interesting feature is a peak at 1743 cm^{-1} with a half-width of 16 cm^{-1} that we ascribe to protonation of Glu 278 based on earlier assignment of a shift around 1740 cm^{-1} to perturbation of this residue (*34*, *35*) and on a ∼4 cm^{-1} shift of the 1743 cm^{-1} band in D_2O experiment (our unpublished observations). Other primary features, peaks at 1659 and 1547 and troughs at 1528 and 1234 cm^{-1}, most likely reflect the conversion of the heme a_3 ferryl state to O_H as judged from their similarity to the static O-minus-F spectrum (*20*, *32*, *33*). One more characteristic band is a trough centered at 1416 cm^{-1}. A similar band was earlier identified in our redox titrations (*36*) and assigned to reduced Cu_A. Several other characteristic bands are marked in Figure 4A.

The concentration of the catalytically active fraction of the mutant enzyme was estimated based on the extinction coefficient of the α-form of the heme a_3−CO complex (4.9 mM^{-1} cm^{-1}, *22*) that is photolyzed in the presence of O_2. It was found to be ∼0.5 mM which is ∼6 times smaller than the redox-active concentration of WT C*c*O (*21*). The small fraction of the catalytically active D124N mutant enzyme is likely due to the tough procedure of the 'ATR-sample' preparation that seems to be even tougher for the mutant C*c*O compared to WT. The latter is concluded from the higher concentration of the Cu_B−CO adduct in the mutant enzyme. According to the extinction coefficient of glutamic acid (*37*), the amplitude of the peak at 1743 cm^{-1} in the O_H-minus-F kinetic spectrum is compatible with complete protonation of a single glutamic acid residue. The trough at

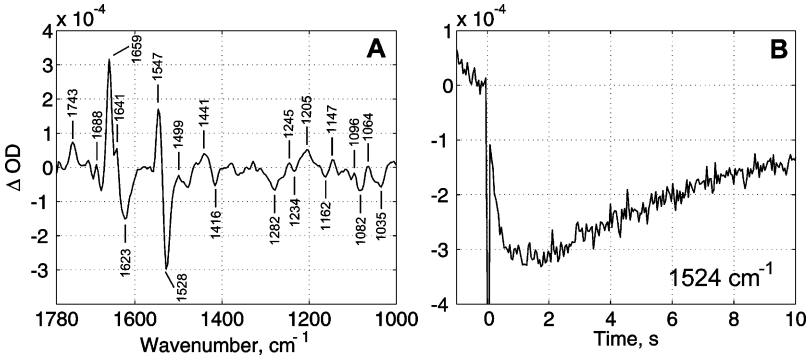

FIGURE 4: FTIR spectrum of the F→O_H transition on D124N mutant C*c*O (A) and its development (B). The kinetic trace in B (1524 cm^{-1}, from averaged FTIR surface) shows development of pretrigger data points, immediate response on laser flash, fast (~400 ms) phase assigned to the F→O_H transition, and slow phase caused by buffer components migration into the ATR-protein film.

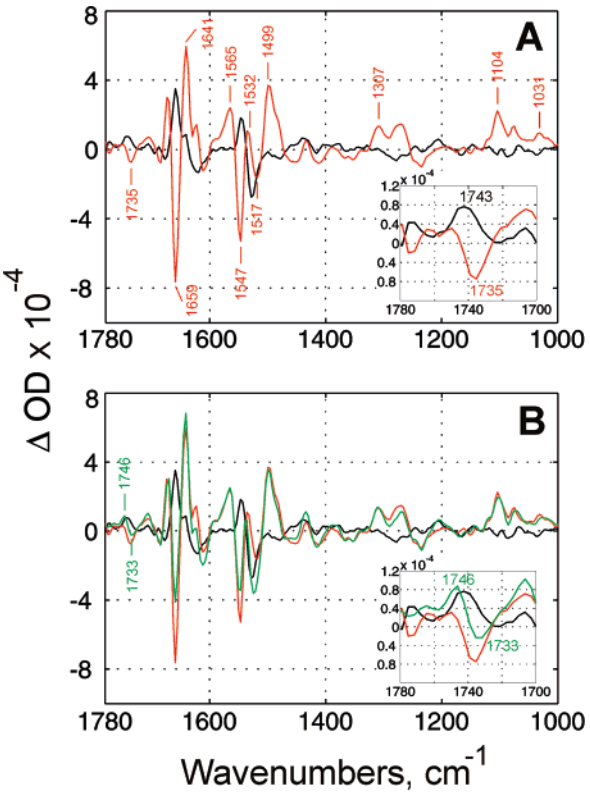

FIGURE 5: Spectra of different kinetic phases of the D124N mutant C*c*O reaction with O_2. (A) O_H-minus-F spectrum (black) is the same as in Figure 4A, red trace is corresponding F-minus-FRCO spectrum with marked main bands. (B) Black and red spectra are from A plotted together with O_H-minus-FRCO (green) that is the sum of F-minus-FRCO and O_H-minus-F spectra. The enlarged view of 1780−1700 cm^{-1} region is shown in the insets.

1416 cm^{-1}, if it belongs to Cu_A oxidation, corresponds to ~70% of full amplitude (from the extinction coefficient defined in ref *21*).

The FRCO→F Transition by FTIR. A 46 ms resolution is not enough to follow the R→P and P→F steps, whose τ values are <80 μs (*4*) and the 35 ms part of the F→O_H phase in the D124N mutated C*c*O. Still, we can get the FRCO-minus-F spectrum (shown in Figure 5A, red spectrum, together with O_H-minus-F spectrum in black), with possible contamination by the fast F→O_H component, by subtracting the spectrum obtained immediately after the laser flash from the spectrum taken before. The correction of the kinetic F→O_H FTIR spectrum by the fast F→O_H part of reaction (if it would have the same infrared signatures as the 400 ms part) did not change the band positions in the spectrum of the FRCO→F transition (not shown).

The most interesting feature of the FRCO→F spectrum is a trough at 1735 cm^{-1} that is the counterpart of the peak at 1743 cm^{-1} in the F→O_H spectrum. Both of these bands have about equal amplitudes and the same band-shift in D_2O (unpublished observations). Since we detected the disappearance/appearance of the bands rather than their shift, our data very likely suggest deprotonation of Glu 278 in the P→F and its reprotonation in the F→O_H transition. Other major bands of the FRCO→F spectrum (see Figure 5A) most likely reflect heme vibrations caused by redox and ligand changes in the binuclear center. In addition, three bands of Cu_B oxidoreduction (*36*) are present in the F-minus-FRCO spectrum with positions at 1307, 1104, and 1031 cm^{-1} (see Figure 5A), reflecting disappearance of reduced Cu_B.

The Kinetic FRCO→O_H Spectrum. The kinetic O_H-minus-FRCO IR spectrum of D124N mutant C*c*O (Figure 5B, green trace) was obtained as a sum of the O_H-minus-F and F-minus-FRCO spectra. The kinetic O_H-minus-FRCO spectrum of the D124N mutant enzyme contains similar main features as the equilibrium O-minus-R spectrum of the WT enzyme (see for example refs *20*, *36*, *38*). Note especially the well-described 1746/1733 cm^{-1} shift assigned to an H-bonding change of protonated Glu 278, which is marked in Figure 5B.

Representative FTIR Kinetic Traces at Specific Wavenumbers. Kinetic traces of the oxygen reaction at specific wavenumbers are plotted in Figure 6. Each trace consists of several points of pretrigger data (before the laser flash), laser spike, jump, and the kinetic phase with τ ~400 ms assigned to the F→O_H reaction step.

Figure 6A shows the kinetic trace at 1739 cm^{-1} that is assigned to deprotonation of Glu 278 in the FRCO→F step and its reprotonation in the F→O_H. At this wavenumber both bands (the trough at 1735 cm^{-1} in the spectrum of the FRCO→F and the peak at 1743 cm^{-1} in the spectrum of the F→O_H reactions) have almost equal amplitudes (see Figure 5A, inset).

In Figure 6B the same trace is shown as in Figure 4B, but with subtracted slow phases and pretrigger drift, and are likely to reflect binuclear center F→O_H conversion (*20*, *33*, *39*) together with disappearance of deprotonated Glu 278. The amplitudes of two prominent bands at 1659 (Figure 6C) and 1547 (Figure 6D) cm^{-1}, that were assigned to heme *a* vibrations (*36*), first, drop down in the fast unresolved phase

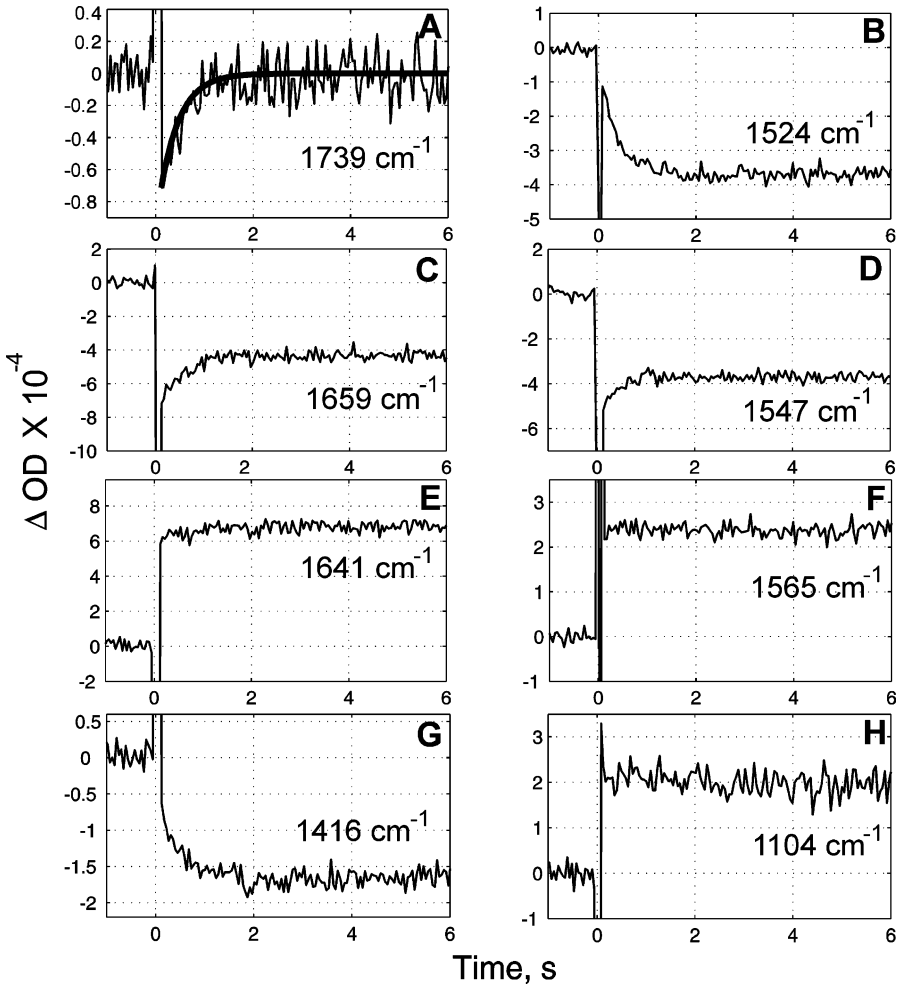

FIGURE 6: (A-H) Representative FTIR kinetic traces of oxygen reaction on D124N mutant C*c*O. Oxygen reaction starts at 0 time with laser flash; kinetics were cut off at 6 s in the figures. The slow kinetic phases due to the buffer components diffusion are defined (τ and amplitude) at each of the shown wavenumbers by SPLMOD fit procedure and subtracted. Pretrigger data drift was subtracted as well. The trace in A is plotted together with theoretical exponential curve of 400 ms time constant.

and then rise up to ~40% of the drop amplitude in the 400 ms phase. This behavior is too complicated to be ascribed simply to heme *a* oxidoreduction. These bands reflect not only the redox status of electron-transfer centers but also ligand exchange in the binuclear site. For example, CO photolysis from FRCO (see ref *14* for *P. denitrificans* data) affects these bands even if there are no redox reactions but only ligand release from the binuclear center.

Development of the main heme a_3 bands at 1641 and 1565 cm^{-1} (*36*) is plotted in Figure 6E and 6F, respectively. The amplitude of these bands is increasing in the fast unresolved phase almost without further changes in the 400 ms F→O_H phase. The kinetics at these wavenumbers reflects the consequence of unresolved processes: FRCO photolysis followed by the P→F reaction and the fast part of the F→O_H transition. During the 400 ms F→O_H phase, these bands are changing only slightly.

The development of the band at 1416 cm^{-1} is shown in Figure 6G and includes a fast unresolved drop followed by a 400-ms decrease. The kinetics may be explained by fractional oxidation of Cu_A in the 35 ms F→O_H phase with further slow final oxidation. However, this band may partly belong to the asymmetric stretch of deprotonated Glu 278 (see below).

The kinetics of Cu_B oxidoreduction is presented in Figure 6H by the example of the 1104 cm^{-1} band. All these changes happened immediately after the laser flash, which is consistent with disappearance of the reduced form of Cu_B.

DISCUSSION

Glutamic acid 278 is a one of the major players in electron-coupled proton transfer in aa_3-type cytochrome *c* oxidases. It takes protons from the N-side of the membrane and delivers them to the oxygen-binding site or to the pump site. The D124N mutation blocks the entry to the proton-conductive D-channel that leads to Glu 278 and is hence expected to decelerate reprotonation of Glu 278 (*8*). The mutation slowed down the F→O_H transition and thus allowed us to measure it by rapid-scan FTIR. Electron flow from Cu_A to the binuclear center was suggested to be limited by the reprotonation of Glu 278 (*8*), and indeed the possible spectral feature of Cu_A oxidation, as well as features of the F→O_H conversion, appeared in the spectrum with the same time constant (~400 ms) as the reprotonation of Glu 278.

We detected reprotonation of Glu 278 in the F→O_H transition with a peak position at 1743 cm^{-1} and its prior deprotonation in the FRCO→F step with a trough at 1735 cm^{-1}. The amplitude of the 1743 cm^{-1} band corresponds to

uptake of about one proton by the glutamate in the 400 ms phase.

Although recent theoretical work on proton transfer in the D-channel (*40*, *41*) predicted that Glu 278 could not be deprotonated for energetic reasons, our results prove its deprotonation during catalytic turnover of the mutant enzyme studied.

We conclude that the 1746/1733 cm^{-1} shift in the O_H-minus-FRCO, as well as in the equilibrium O-minus-R spectra, is due to different strengths of H-bonding of protonated Glu 278 in the oxidized and reduced states, which is shown here by the different band positions of Glu 278 deprotonation in the P→F and its reprotonation in the F→O_H step. The H-bond is stronger in the reduced state, as it is seen from the different position of the bands, which reinforces the earlier conclusions of an environmental change around the protonated Glu 278 (*16*, *42*).

Even if infrared features of the transient F→O_H spectrum in the amide regions resemble those in the equilibrium spectrum (*20*, *33*, *39*), the shape of the bands differs. The trough at 1528 cm^{-1}, that is present in the equilibrium spectrum as well, but different in shape, can be the result of overlapping bands of the binuclear center conversion with those of the antisymmetric mode of deprotonated Glu 278. The corresponding peak reflecting deprotonation of Glu 278 in the F-minus-FRCO spectrum may be the one centered at around 1532 cm^{-1} and marked in Figure 5A. The peak at 1515 cm^{-1} (assigned to protonated Y280 in O state (*39*)) in the equilibrium spectra cannot be seen in the kinetic F→O_H spectrum of the D124N mutant. One possible reason is a masking effect from a trough of the antisymmetric stretch of deprotonated Glu 278 that is expected to be located in this region. Another assumption is based on a difference between O_H and O states. Tyr 280 was expected to be deprotonated in the F state and to stay deprotonated in the next O_H state (*1*). Our speculation is that deprotonated Tyr-280 may take a proton from outside the enzyme upon relaxation of the transient oxidized state O_H into O, since the possible signature of protonated Tyr could be seen only in the equilibrium spectrum in the relaxed O state (*39*).

The trough at 1416 cm^{-1}, observed in the kinetic O_H-minus-F spectrum and absent in the equilibrium spectrum, may reflect Cu_A oxidoreduction or the symmetric mode of deprotonated Glu 278.

In the present work we applied kinetics of the oxygen reaction measurements on the D124N mutant of cytochrome *c* oxidase by FTIR. The ATR-approach allowed initiation of the oxygen reaction a number of times on the same immobilized enzyme. Although only a small fraction (∼15−20%) of the D124N mutant enzyme was catalytically active, its activity and stability on the ATR prism was retained after more than 100 O_2 injections and laser flashes, which serves as a good basis for further kinetic studies.

REFERENCES

1. Wikström, M., and Verkhovsky, M. I. (2007) Mechanism and energetics of proton translocation by the respiratory heme-copper oxidases, *Biochim. Biophys. Acta 1767*, 1200−1214.
2. Bloch, D., Belevich, I., Jasaitis, A., Ribacka, C., Puustinen, A., Verkhovsky, M. I., and Wikström, M. (2004) The catalytic cycle of cytochrome c oxidase is not the sum of its two halves, *Proc. Natl. Acad. Sci. U.S.A. 101*, 529−533.
3. Wikström, M., and Verkhovsky, M. I. (2006) Towards the mechanism of proton pumping by the haem-copper oxidases, *Biochim. Biophys. Acta 1757*, 1047−1051.
4. Belevich, I., Verkhovsky, M. I., and Wikström, M. (2006) Proton-coupled electron transfer drives the proton pump of cytochrome c oxidase, *Nature 440*, 829−832.
5. Iwata, S., Ostermeier, C., Ludwig, B., and Michel, H. (1995) Structure at 2.8-Angstrom resolution of cytochrome c oxidase from *Paracoccus denitrificans*, *Nature 376*, 660−669.
6. Verkhovskaya, M. L., GarciaHorsman, A., Puustinen, A., Rigaud, J. L., Morgan, J. E., Verkhovsky, M. I., and Wikström, M. (1997) Glutamic acid 286 in subunit I of cytochrome bo_3 is involved in proton translocation, *Proc. Natl. Acad. Sci. U.S.A. 94*, 10128−10131.
7. Ädelroth, P., Ek, M. S., Mitchell, D. M., Gennis, R. B., and Brzezinski, P. (1997) Glutamate 286 in cytochrome aa_3 from *Rhodobacter sphaeroides* is involved in proton uptake during the reaction of the fully-reduced enzyme with dioxygen, *Biochemistry 36*, 13824−13829.
8. Smirnova, I. A., Ädelroth, P., Gennis, R. B., and Brzezinski, P. (1999) Aspartate-132 in cytochrome c oxidase from *Rhodobacter sphaeroides* is involved in a two-step proton transfer during oxo-ferryl formation, *Biochemistry 38*, 6826−6833.
9. Gerwert, K., Souvignier, G., and Hess, B. (1990) Simultaneous monitoring of light-induced-changes in protein side-group protonation, chromophore isomerization, and backbone motion of bacteriorhodopsin by time-resolved Fourier-transform infrared-spectroscopy, *Proc. Natl. Acad. Sci. U.S.A. 87*, 9774−9778.
10. Zscherp, C., Schlesinger, R., Tittor, J., Oesterhelt, D., and Heberle, J. (1999) In situ determination of transient pK_a changes of internal amino acids of bacteriorhodopsin by using time-resolved attenuated total reflection Fourier-transform infrared spectroscopy, *Proc. Natl. Acad. Sci. U.S.A. 96*, 5498−5503.
11. Garczarek, F., and Gerwert, K. (2006) Functional waters in intraprotein proton transfer monitored by FTIR difference spectroscopy, *Nature 439*, 109−112.
12. Remy, A., and Gerwert, K. (2003) Coupling of light-induced electron transfer to proton uptake in photosynthesis, *Nature Struct. Biol. 10*, 637−644.
13. Ritter, E., Elgeti, M., Hofmann, K. P., and Bartl, F. J. (2007) Deactivation and proton transfer in light-induced metarhodopsin II/ metarhodopsin III conversion: a time-resolved Fourier transform infrared spectroscopic study, *J. Biol. Chem. 282*, 10720−10730.
14. Rost, B., Behr, J., Hellwig, P., Richter, O. M. H., Ludwig, B., Michel, H., and Mäntele, W. (1999) Time-resolved FT-IR studies on the CO adduct of *Paracoccus denitrificans* cytochrome c oxidase: Comparison of the fully reduced and the mixed valence form, *Biochemistry 38*, 7565−7571.
15. Heitbrink, D., Sigurdson, H., Bolwien, C., Brzezinski, P., and Heberle, J. (2002) Transient binding of CO to Cu-B in cytochrome c oxidase is dynamically linked to structural changes around a carboxyl group: A time-resolved step-scan Fourier transform infrared investigation, *Biophys. J. 82*, 1−10.
16. Bailey, J. A., Tomson, F. L., Mecklenburg, S. L., MacDonald, G. M., Katsonouri, A., Puustinen, A., Gennis, R. B., Woodruff, W. H., and Dyer, R. B. (2002) Time-resolved step-scan Fourier transform infrared spectroscopy of the CO adducts of bovine cytochrome c oxidase and of cytochrome bo_3 from *Escherichia coli*, *Biochemistry 41*, 2675−2683.
17. Koutsoupakis, C., Soulimane, T., and Varotsis, C. (2003) Ligand binding in a docking site of cytochrome c oxidase: A time-resolved step-scan Fourier transform infrared study, *J. Am. Chem. Soc. 125*, 14728−14732.
18. Riistama, S., Laakkonen, L., Wikström, M., Verkhovsky, M. I., and Puustinen, A. (1999) The calcium binding site in cytochrome aa_3 from *Paracoccus denitrificans*, *Biochemistry 38*, 10670−10677.
19. Vakkasoglu, A. S., Morgan, J. E., Han, D., Pawate, A. S., and Gennis, R. B. (2006) Mutations which decouple the proton pump of the cytochrome c oxidase from *Rhodobacter sphaeroides* perturb the environment of glutamate 286, *FEBS Lett. 580*, 4613−4617.
20. Iwaki, M., Puustinen, A., Wikström, M., and Rich, P. R. (2003) ATR-FTIR spectroscopy of the P-M and F intermediates of bovine and *Paracoccus denitrificans* cytochrome c oxidase, *Biochemistry 42*, 8809−8817.

21. Gorbikova, E. A., Belevich, N. P., Wikström, M., and Verkhovsky, M. I. (2007) Protolytic reactions on reduction of cytochrome c oxidase studied by ATR-FTIR spectroscopy, *Biochemistry 46*, 4177−4183.
22. Yoshikawa, S., Choc, M. G., Otoole, M. C., and Caughey, W. S. (1977) IR study of CO binding to heart cytochrome c oxidase and hemoglobin A. Implications of re O_2 reactions, *J. Biol. Chem. 252*, 5498−5508.
23. Provencher, S. W., and Vogel, R. H. (1983) Regularization Techniques for Inverse Problems in Molecular Biology, *Progress in Scientific Computing* (Deufhard, E., Hairer, E., Eds.) pp 304−319, Birkhauser, Boston.
24. Morgan, J. E., Verkhovsky, M. I., Puustinen, A., and Wikström, M. (1995) Identification of a peroxy intermediate in cytochrome bo_3 of *Escherichia coli*, *Biochemistry 34*, 15633−15637.
25. Park, S., Pan, L. P., Chan, S. I., and Alben, J. O. (1996) Photoperturbation of the heme a_3-Cu-B binuclear center of cytochrome c oxidase CO complex observed by Fourier transform infrared spectroscopy, *Biophys. J. 71*, 1036−1047.
26. Fiamingo, F. G., Altschuld, R. A., and Alben, J. O. (1986) Alpha and beta forms of cytochrome-c-oxidase observed in rat-heart myocytes by low-temperature Fourier-transform infrared-spectroscopy, *J. Biol. Chem. 261*, 2976−2987.
27. Belevich, I., Tuukkanen, A., Wikström, M., and Verkhovsky, M. I. (2006) Proton-coupled electron equilibrium in soluble and membrane-bound cytochrome c oxidase from *Paracoccus denitrificans*, *Biochemistry 45*, 4000−4006.
28. Sigurdson, H., Branden, M., Namslauer, A., and Brzezinski, P. (2002) Ligand binding reveals protonation events at the active site of cytochrome c oxidase; is the K-pathway used for the transfer of H^+ or OH^-, *J. Inorg. Biochem. 88*, 335−342.
29. Wikström, M. (1981) Energy-dependent reversal of the cytochrome-oxidase reaction, *Proc. Natl. Acad. Sci. U.S.A. 78*, 4051−4054.
30. Witt, S. N., Blair, D. F., and Chan, S. I. (1986) Chemical and spectroscopic evidence for the formation of a ferryl Fea_3 intermediate during turnover of cytochrome-c-oxidase, *J. Biol. Chem. 261*, 8104−8107.
31. Ribacka, C., Verkhovsky, M. I., Belevich, I., Bloch, D. A., Puustinen, A., and Wikström, M. (2005) An elementary reaction step of the proton pump is revealed by mutation of tryptophan-164 to phenylalanine in cytochrome c oxidase from *Paracoccus denitrificans*, *Biochemistry 44*, 16502−16512.
32. Nyquist, R. M., Heitbrink, D., Bolwien, C., Gennis, R. B., and Heberle, J. (2003) Direct observation of protonation reactions during the catalytic cycle of cytochrome c oxidase, *Proc. Natl. Acad. Sci. U.S.A. 100*, 8715−8720.
33. Pereira, M. M., Sousa, F. L., Teixeira, M., Nyquist, R. M., and Heberle, J. (2006) A tyrosine residue deprotonates during oxygen reduction by the caa_3 reductase from Rhodothermus marinus, *FEBS Lett. 580*, 1350−1354.
34. Puustinen, A., Bailey, J. A., Dyer, R. B., Mecklenburg, S. L., Wikström, M., and Woodruff, W. H. (1997) Fourier transform infrared evidence for connectivity between Cu-B and glutamic acid 286 in cytochrome bo_3 from *Escherichia coli*, *Biochemistry 36*, 13195−13200.
35. Hellwig, P., Behr, J., Ostermeier, C., Richter, O. M. H., Pfitzner, U., Odenwald, A., Ludwig, B., Michel, H., and Mäntele, W. (1998) Involvement of glutamic acid 278 in the redox reaction of the cytochrome c oxidase from *Paracoccus denitrificans* investigated by FTIR spectroscopy, *Biochemistry 37*, 7390−7399.
36. Gorbikova, E. A., Vuorilehto, K., Wikström, M., and Verkhovsky, M. I. (2006) Redox titration of all electron carriers of cytochrome c oxidase by Fourier transform infrared spectroscopy, *Biochemistry 45*, 5641−5649.
37. Venyaminov, S. Yu., and Kalnin, N. N. (1990) Quantitative IR spectrophotometry of peptide compounds in water (H_2O) solutions. I. Spectral parameters of amino acid residue absorption bands, *Biopolymers 30*, 1243−1257.
38. Hellwig, P., Rost, B., Kaiser, U., Ostermeier, C., Michel, H., and Mäntele, W. (1996) Carboxyl group protonation upon reduction of the Paracoccus denitrificans cytochrome c oxidase: Direct evidence by FTIR spectroscopy, *FEBS Lett. 385*, 53−57.
39. Nyquist, R. M., Heitbrink, D., Bolwien, C., Gennis, R. B., and Heberle, J. (2003) Direct observation of protonation reactions during the catalytic cycle of cytochrome c oxidase, *Proc. Natl. Acad. Sci. U.S.A. 100*, 8715−8720.
40. Olsson, M. H. M., Sharma, P. K., and Warshel, A. (2005) Simulating redox coupled proton transfer in cytochrome c oxidase: Looking for the proton bottleneck, *FEBS Lett. 579*, 2026−2034.
41. Xu, J. C., Sharpe, M. A., Qin, L., Ferguson-Miller, S., and Voth, G. A. (2007) Storage of an excess proton in the hydrogen-bonded network of the D-pathway of cytochrome c oxidase: Identification of a protonated water cluster, *J. Am. Chem. Soc. 129*, 2910−2913.
42. Lübben, M., Prutsch, A., Mamat, B., and Gerwert, K. (1999) Electron transfer induces side-chain conformational changes of glutamate-286 from cytochrome bo_3, *Biochemistry 38*, 2048−2056.

BI701614W